MEASUREMENT AND ANALYSIS OF NEAR BED SEDIMENT PROCESSES BY WAVES IN RIPPLED BED AND PLANE BED REGIME

Alireza Ahmari[1] and Hocine Oumeraci[2]

1. Coastal Research Centre (FZK) of Leibniz University of Hannover and Technical University of Braunschweig, Merkurstr 11, 30419 Hannover, Germany.
ahmari@fzk.uni- hannover.de
2. Leichtweiß-Institute for Hydraulic Engineering and Water Resources of Technical University of Braunschweig, Beethovenstr. 51a 38106 Braunschweig, Germany
h.oumeraci@tu-bs.de

Abstract: Sediment transport in coastal zones caused by waves and tides modifies continuously the cross-shore profile and the shape of the coast line. Since the transport of sediments is the result of the interaction between the hydrodynamic forcing (waves, currents) and the sea bed morphology (rippled and plane bed), a high temporal and spatial accuracy of the sediment entrainment above both rippled and plane sea bottom in the near shore zone is crucial to substantially improve the understanding of all processes involved and to come up with more reliable prediction formulae. With this background, the sediment concentration and the seabed profile evolution under regular/irregular non-breaking and near breaking waves were simultaneously measured in large-scale experiments by comparatively using a multi frequency Acoustic Backscattering Technique (ABS), an optical measurement technique (Optical Turbidity Meter) and a mechanical Transverse Suction System (TSS). A comparative analysis of the suspended sediment entrainment above the rippled bed and the plane bed is performed which provides a more precise determination of the reference concentration, the vertical distribution of the suspended sediment concentration and the sediment diffusivity profiles.

Introduction

The entrainment processes of the suspended sediment under non-breaking waves above rippled beds and plane sea beds are fundamentally different (Nielsen, 1992; Thorne and Hanes, 2002). As the sea bed surface in the near shore zone is rarely flat, suspended load as a major part of the total sediment transport over ripples has become one of the most interesting research topics in the field of sediment transport over recent years. In contrast to the dynamically plane bed regime, where the sheet flow is the dominant transport process and the momentum transfer occurs due to the turbulent diffusion, above steep ripples the sediment dynamics within an about 2-3 ripple height thick layer close to the sea bed is dominated by the generation of coherent periodic vortex structures

induced by the flow separation at the steep ripple crests followed by their shedding at the time of the flow reversal. Outside this layer, where the coherent motions break down, turbulent processes dominate and the sand particles are entrained to much higher elevations than above the plane beds.

Moreover, in the case of steep ripples, the major peaks of the suspended concentration above the ripple crest occur just ahead of the flow reversal and the net transport rate will be offshore due to the phase lag between the flow and the suspended concentrations induced by the lee-vortices in a combination with the asymmetry of the waves. Whereas the suspended sediment event above short crested mega ripples or above dynamically plane beds can be described by means of the turbulent diffusion concept, the later cannot be applied to predict the well-organized sediment entrainment processes above the sea beds covered with long crested 2D vortex ripples (Thorne et al. 2003).

In the first part of the paper, a comparative analysis of the temporal and spatial distribution of the suspended sediment concentrations measured by Acoustic Backscattering Technique (ABS) and Optical Turbidity meter is performed. The results of the experiments show that the multi frequency acoustic backscattering technique is obviously a unique measurement technique to describe the temporal and spatial entrainment of the suspended sediment concentration beneath non-breaking waves particularly around steep ripples. The time-averaged measurements of suspended sediment concentration using Transverse Suction System (TSS) are also considered to compare the mean sediment concentration obtained from different measuring techniques.

The second part of the paper focuses on a comprehensive analysis of the entrainment mechanisms of the suspended sediment concentration and sediment diffusivity profiles above rippled and plane bed using the results obtained from large scale experiments recently performed in the Large Wave Flume (GWK). As a result it is proposed to investigate the most important parameters involved in both oscillatory flow due to waves and suspended sediment entrainment over plane and rippled beds. These hydrodynamic and morphodynamic parameters are crucial as they will represent the essential non-dimensional quantities to be used for the description of the temporal and spatial suspended sediment entrainment processes under non- and near breaking waves above rippled- and dynamically plane bed.

Experimental set-up

The large-scale experiments carried out in the Large Wave Flume (GWK) in Hannover aim at the measurement of the sediment entrainment and the vertical

distribution of the suspended sediment concentration in time and space above different bed formations and beneath different waves.

The flume has an effective length of 300 m, a width of 5 m and a depth of 7 m. The experiments were conducted at different locations of the longitudinal beach profile (test groups shown in Fig. 1) with different hydrodynamic conditions, which are briefly summarized in Table 1.

For the experiments, the concrete bottom of the GWK-flume was covered with a sand layer of about 0.82 m thick representing the sea bed made of well-sorted sand (GWK sand) with $d_{50} = 0.242$ mm and a non-uniformity factor of $U = d_{60}/d_{10} = 2.24$ (see Fig. 1).

As can be seen in Fig. 1 (see also Table 1for test conditions), the morphologic and hydrodynamic conditions for group 1 of experiments provide a low energy flow which results in a rippled bed regime under non breaking waves, whereas the conditions for group 2 provide a high energy flow regime associated with a plane bed formation under near breaking waves. Table 2 summarizes the flow regimes tested in terms of the Reynolds number related to the orbital amplitude ($RE=A_0U/\nu$), where A_0 is the orbital amplitude and U the near bed velocity amplitude, and the relative roughness (A_0/k_s), where k_s is the equivalent bed roughness, as well as the bed form characteristics recorded for both groups of experiments.

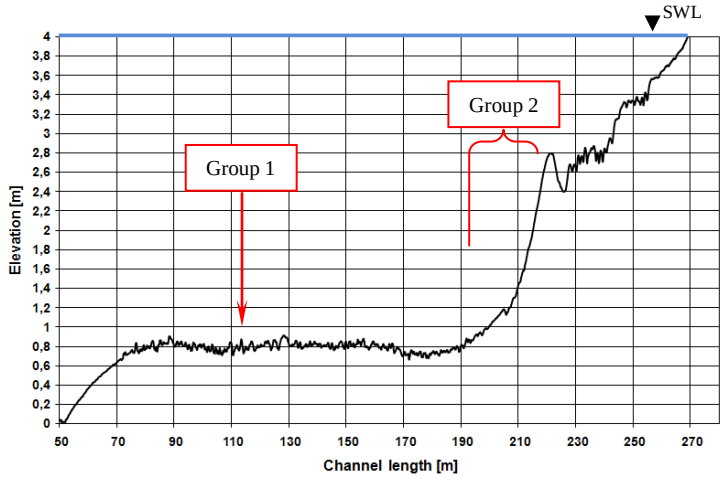

Fig. 1. Beach profile in the Large Wave Flume (GWK)

Table 1. Test conditions in the Large Wave Flume (GWK)

Experiment groups	Waves	Wave asymmetry (u_c/u_t)	h (m)	H, H_s (m)	T, T_p (s)
Group 1	Symmetric to weekly asymmetric non- breaking regular waves and irregular waves (JONSWAP-spectra)	0.87-1.00	3.20	0.8-1.2	5
Group 2	Strong asymmetric near breaking regular waves and irregular waves (JONSWAP-spectra)	1-1.42	3.0 -1.26	0.8-1.0	7, 5

h: Water depth, H: Height of regular wave, H_s: Significant height of irregular waves, T: Period of regular waves, T_p: Peak period of irregular waves, u_c: Wave crest velocity, u_t: Wave trough velocity

Table 2. Flow regimes and bed form characteristics for both groups of experiments.

Experiment groups	Reynolds number, (RE_{A0})	Relative roughness, (A_0/k_s)	Boundary layer flow regime	Ripple steepness, (η_r/λ_r)	Bed characteristics
Group 1	O (10^5)	O (1-3)	Low energy flow	0.10-0.14	Well developed 2D ripples
Group 2	O (10^6)	O (4-10)	High energy flow	-	Dynamically plane bed

Suspended sediment concentration recorded above the sea bed

Group 1 of large-scale experiments in GWK were performed under non-breaking waves, where suspended load above 2D and 3D ripples is dominant. The ABS was used to capture the time-varying suspended sediment concentration profiles above the sea bed. To compare the suspended concentration time series at given elevations above the sea bottom, four pieces of Optical Turbidity Meter were also fixed at the same measuring station. Using the time averaged concentrations obtained by Transverse Suction System (TSS), recorded within the time period of 20 min during each test, provided comparable mean concentration values with those calculated by means of the ABS data set.

The grain size distribution of suspended sediment concentration captured by TSS was also used to obtain the sediment diffusivity profiles above the sea bed.

Fig. 2 represents exemplarily a comparison between time- and bed- averaged Suspended Sediment Concentration (SSC) above rippled and plane beds under different wave conditions measured by acoustical, optical and mechanical devices, showing a good agreement between the results calculated with the ABS-data set and those measured by the Optical Turbidity Meter and TSS.

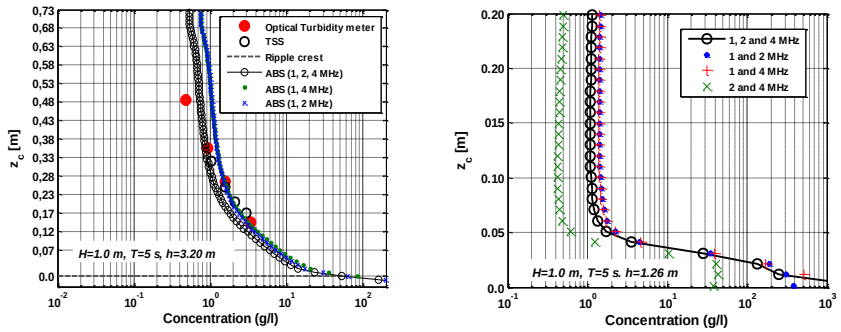

a) SSC above rippled bed

b) SSC above dynamically plane bed

Fig. 2. Time- and bed-averaged concentration: Concentration profiles measured by ABS (1, 2 and 4 MHz transducers); Concentration points measured by Optical Turbidity meter (red circles) and by TSS (closed white circles) for a) group 1 of experiments above rippled bed under non-breaking regular waves. b) group 2 of experiments above dynamically plane bed under near breaking regular waves (see also Fig. 1).

Fig. 3-a,b show a time window of suspended sediment entrainment around a steep vortex ripple (η_r/λ_r = 0.12) under non-breaking weekly asymmetric regular waves (test conditions: H= 1.0 m, T= 5 s, h/L= 0.125) and above a dynamically plane bed (η_r/λ_r = 0) just before wave breaking point under strong asymmetric near breaking regular waves (test conditions: H=1.0 m, T= 5 s, h/L= 0.075), respectively, including horizontal orbital flow velocity u, measured with an Electromagnetic Current Meter (ECM) at 0.25 m above the undisturbed sea bed (the panels on the top in Fig. 3) in both cases. The suspended concentrations at different locations of the bed evolution time series beneath ABS were combined to generate the images.

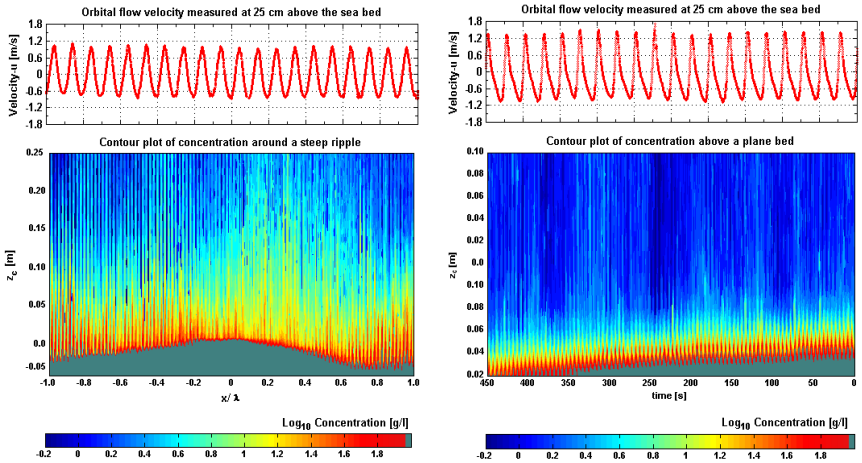

a) SSC above rippled sea bed b) SSC above plane sea bed

Fig. 3. Horizontal orbital flow velocity *u*, and Suspended Sediment Concentration (SSC), above (a) a steep ripple beneath non breaking weekly asymmetric regular waves and (b) a plane bed beneath near breaking strong asymmetric regular waves. The colors in the contour plot are defined in the color bar as "Log_{10} (Concentration in g/l)".

Phase- and bed dependent concentration around a steep ripple

The suspended concentration around a steep 2D-ripple is determined for 10 selected phase angles of each wave cycle as shown in Fig. 4.

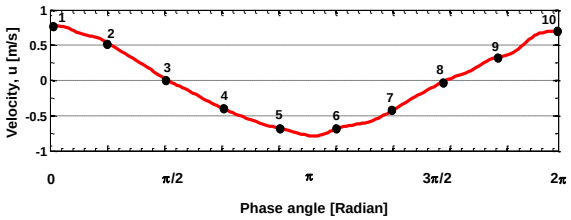

Fig.4. Wave induced horizontal orbital velocity at 10 selected phase angles of a wave cycle

As a result the details of the intra wave concentration event determined over a time period of 450 s (90 successive non breaking regular waves), i.e. as the ripple passed on-shore directed beneath ABS, are obtained in Fig.5. Each suspended concentration contour pattern (panels 1 to 10) represents the suspended concentration entrainment for the different phase angles shown in Fig.4. As can be seen in Fig. 5, the high sediment entrainment occurred at the lee slope of the migrated ripple, which takes place in the time of the maximum positive flow velocity (points 1 and 2 in Fig. 4, $0< \varphi <\pi/4$, where φ is the phase angle).

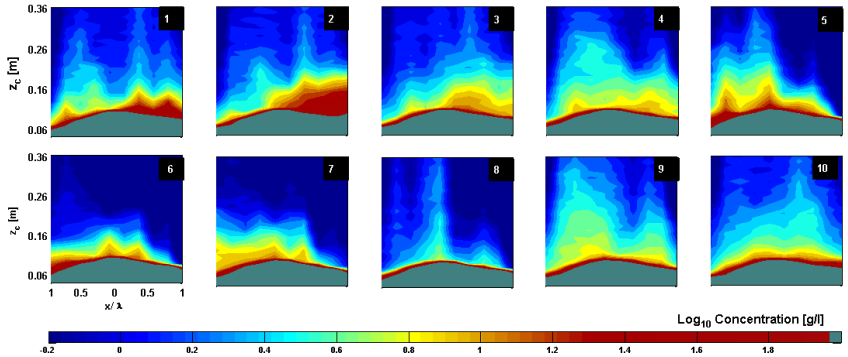

Fig. 5. Sound imaging of vortex generations and suspended sediment entrainment over a ripple under non-breaking regular waves. The numbers indicate the selected phases of the wave cycle as depicted in Fig. 4

When the forward flow reduces in strength (point 3 in Fig. 4, $\varphi = \pi/2$), the horizontal component of the orbital velocity reduces to zero and the vertical component of the orbital velocity is directed upwards and maximum near the sea bed (Ahmari and Oumeraci, 2010). This later causes the sediment-laden vortex to move up the on-shore slope of the ripple towards the ripple crest and causes an ejection of the suspended sediment clouds upwards into the water column (see Fig.4 points 3,4 and Fig. 5, panels 3 and 4).

As the flow reverses, the sediment-rich lee vortex generated at the off-shore slope of the ripple moves over the ripple crest and begins to be shed. At this time, the second vortex is formed at the opposite ripple flank. It can clearly be seen that this vortex is significantly smaller than the first one generated at the on-shore ripple slope, which is due to the asymmetry of the regular waves with H/L=0.04 (see Fig. 4 points 5, 6,7 and Fig.5 concentration panels 5, 6, 7).

Point 8 in Fig.4 represents the second zero crossing ($\varphi=3\pi/2$), where the horizontal component of the orbital velocity becomes zero (Ahmari and Oumeraci, 2010). Looking into the suspended concentration contour pattern (Fig.5, concentration pattern 8) shows that at this point, the concentration event around the ripple is at the lowest rate. From point 8 in Fig.4, the flow begins to reverse again and in point 9 ($\varphi=7\pi/4$) the on-shore directed positive flow increases in strength and becomes maximum at point 10. Correspondingly, the lee vortex on the on-shore flank of the ripple begins to be formed again, which can be observed in Fig.5 (concentration panels 9 and 10).

Sediment diffusivity profiles above rippled bed under non-breaking waves

As shown above in the case of the rippled bed regime, the lee side of the ripples substantially contribute to the periodic intra wave flow velocity and the vortex generation processes, which represent the primary entrainment process of the sand particles into the water column over the ripples.

According to Thorne et al. (2009), the time averaged sediment balance above ripples can be expressed as follows:

$$-w_s C + \overline{w_p C_p} - \varepsilon \frac{dC}{dz} = 0 \quad (1)$$

where C is the suspended sediment concentration, C_p the periodic suspended sediment, w_p the periodic wave-induced near bed flow velocity, $\overline{w_p C_p}$ the vertical upward sediment flux and ε the sediment diffusivity.

Thorne et al. (2009) absorbed the convective transfer term, $\overline{w_p C_p}$, into the "convective diffusivity" term and defined the sediment diffusivity as follows:

$$\varepsilon = \frac{-w_s C}{dC/dz} \quad (2)$$

where w_s is the settling velocity according to Soulsby (1997):

$$w_s = \frac{\upsilon}{d_{50s}} \lfloor (10.36^2 + 1.049 D_*^3)^{0.5} - 10.36 \rfloor \quad (3)$$

and the dimensionless grain size, D_* reads:

$$D_* = d_{50} \left[\frac{(s-1)g}{\upsilon^2} \right]^{1/3} \quad (4)$$

where s is the relative sediment density (s= ρ_s/ρ); g the acceleration due to gravity and υ the kinematic viscosity of water.

To represent the trends in sediment diffusivity, the sediment diffusivity profiles were normalized using the following scaling (for more details see Thorne, et al. 2009):

$$\varepsilon_s / U k_s \text{ with } z/k_s \quad (5)$$

Accorting to the suggestion of Thorne et al. (2002; 2009), the equivalent bed roughness, k_s, above the sea bed covered with steep 2D ripples has been taken as follows:

$$k_s = 25\eta_r(\eta_r/\lambda_r) \quad (6)$$

where η_r and λ_r represent the ripple height and ripple length, respectively. Fig. 6-a shows all of the calculated normalized sediment diffusivity profiles performed in group 1 of experiments (see also Table 1) with normalized heights above the sea bed (gray dots) including the mean sediment diffusivity profile (dark circles).

The normalized sediment diffusivity is constant in a region below the normalized height of z/k_s= 1.2 (Layer 1 in Fig. 6-a), which begins to increase linearly above this elevation (Layer 2 in Fig. 6-a). Observation of the sediment diffusivity increase represented in Fig. 6-a and b shows that above layer 2 (z/k_s > 3) the sediment diffusivity increase becomes less clear. This ambiguity occurs because of the increasing scatter due to the low-concentration level at higher elevations above the sea bed (Thorne et al., 2009).

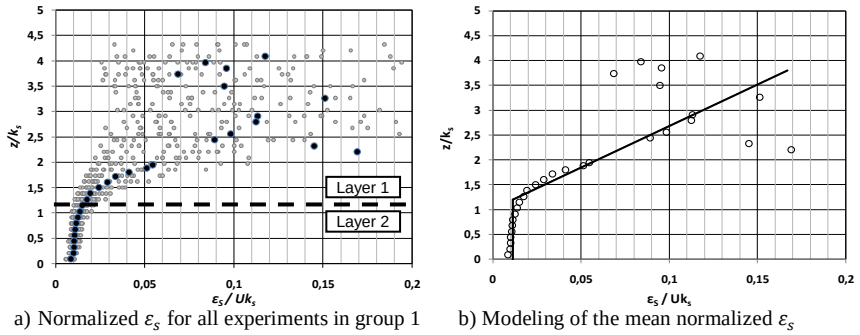

a) Normalized ε_s for all experiments in group 1 b) Modeling of the mean normalized ε_s

Fig. 6. a) Calculation of the normalized sediment diffusivity (ε_s/Uk_s) with normalized height above the sea bed (z/k_s) under regular waves (H= 0.8-1.2 m, T=5 s, h≈3.18 m). b) Mean measured normalized sediment diffusivity and the lines fitted to the mean diffusivity profile above a rippled bed under non-breaking regular waves.

Fig. 6-b shows an empirical relation fitted to the mean sediment diffusivity profiles for measurements under regular waves, which provides an explanation of the sediment diffusivity variation with height above the sea bed as follows:

$$\varepsilon_s = \xi_1 U k_s \quad z \leq 1.2k_s \quad (7)$$

$$\varepsilon_s = \xi_2 U(z - k_s) \quad z > 1.2k_s \quad (8)$$

Where U is the near bed velocity amplitude, $\xi_1 = 0.0112$ and $\xi_2 = 0.06$.

Phase- and bed dependent concentration above plane bed

The suspended concentration over the sea bed just before the wave breaking event is determined for 10 selected phase angles of each wave cycle as shown in Fig. 7.

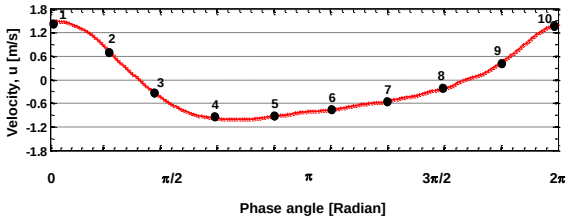

Fig. 7. Wave induced horizontal orbital velocity at 10 selected phase angles of a wave cycle

Fig. 8 shows the details of the suspended concentration event constructed over a time period of 400 s (80 successive near breaking asymmetric regular waves) as the bed profile passed on-shore directed beneath ABS. Each suspended concentration contour pattern in Fig. 8 (panels 1 to 10) represents the suspended concentration entrainment for the phase angles 1 to 20 shown in Fig.7.

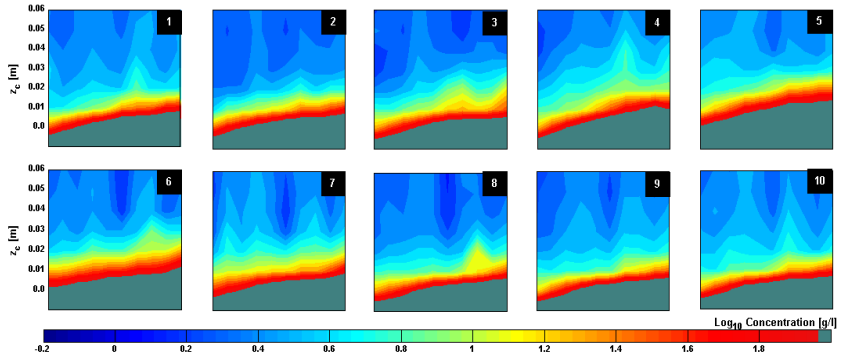

Fig. 8. Sound imaging of sediment entrainment above dynamically plane bed under near-breaking regular waves. The numbers indicate the selected phases of the wave cycle as depicted in Fig. 7

Looking into the concentration panels shows that there is no significant sediment entrainment event, when the flow reverses, as it was the case in a rippled bed regime under non-breaking waves. The large concentrations which are confined to a relative thin layer within a few centimeters over the sea bed (sheet flow) and the variation in the suspended load seems to be only weakly dependent on the wave phase. The concentration panels shown in Fig. 8 indicate

that due to the strong asymmetry of the near-breaking waves close to the bar (test conditions: H=1.0 m, T= 5 s and H/L= 0.07, h/L= 0.075), the ripples are completely washed out. Under such a storm wave situation, the sediment entrainment is not caused by vortex formation. In this case, near bed turbulent flow processes dominate and the transport mode rather corresponds to sheet flow. As the turbulent eddies above a plane bed are considered to grow with the elevation above the sea bed (Davies and Villaret, 1997), the sediment diffusivity increases linearly above the sea bottom, which will be discussed in the following.

Sediment diffusivity profiles above plane bed under near-breaking waves

The same methodology as in the case of a rippled bed regime is applied here to capture the sediment diffusivity under near-breaking waves above the dynamically plane bed. Fig. 9-a shows the normalized sediment diffusivity (ε_s/Uk_s) with normalized height above the sea bed (z/k_s) and Fig. 9-b shows the line fitted to the mean normalized sediment diffusivity. As can clearly be seen here, in contrast to the rippled bed regime, there is no consistent diffusivity close to the plane bed (which is obviously associated with the vortex generation around steep ripples) and the normalized sediment diffusivity increase linearly with normalized height above the sea bed.

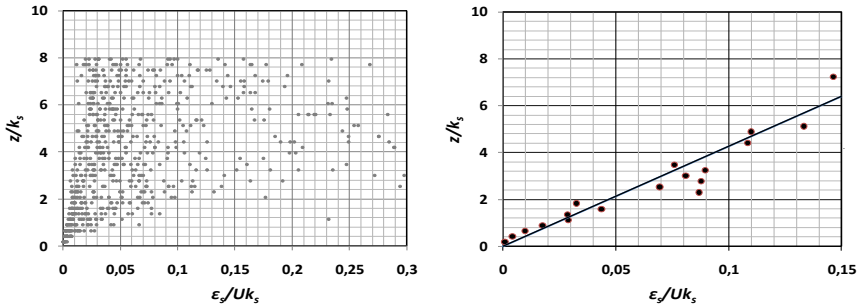

a) Normalized ε_s for all experiments in group 2 b) Modeling of the mean normalized ε_s

Fig. 9. a) Calculation of the normalized sediment diffusivity (ε_s/Uk_s) with normalized height above the plane sea bed (z/k_s) under near-breaking regular waves (H= 0.8-1.0 m, T=5 s, h≈3-1.26 m). b) Mean measured normalized sediment diffusivity and the line fitted to the mean diffusivity profile above a plane bed under near-breaking regular waves.

Finally, the empirical relation for the mean sediment diffusivity behaviour above dynamically plane bed under near breaking waves (H=0.8-1.0 m, T= 5s, h= 1,26-3 m) reads:

$$\varepsilon_s = \psi U z \tag{9}$$

where U is the near bed velocity amplitude and $\psi = 0.023$.

Discussion

The goal of the present paper was to achieve better understanding of the behavior of the sediment entrainment mechanism related to the hydro- und morphodynamic conditions for two important flow regimes in the near shore zone, namely in a low energy flow regime (h/L=0.125, h/H=2.66-4) over a rippled bed under weakly asymmetric regular and irregular non-breaking waves and in a high energy flow regime (h/L=0.07, h/H=1.26-1.57) over a dynamically plane bed beneath strong asymmetric near-breaking regular and irregular waves (see also Tables 1&2 and Fig. 1). According to the observations of Thorne et al. (2009), the variation of the sediment entraiment and the sediment diffusivity profiles over two bed material classified as "medium" and "fine" under slightly asymmetric regular waves, are significantly influenced by the grain size. Under the low enrgy flow conditions, the sea bed composed of coarse sand is fully covered with 2D steep vortex ripples, whereas under the same hydrodynamic conditions, the sea bed composed of fine sand behaved dynamically more like a plane bed, which indicates the importance of the effect of the grain size distribution of the bed material on the sea bed regime , and thus for the prediction of the suspended sediment entrainment in the near shore zone.

These observtions and the detailed results of the current study on suspended sediment entrainment processes suggest that non-dimensional hydro- and morphodynamic parameters are required to describe both in time and space the sediment entrainment mechanisms above different bed forms under different wave conditions. A first attempt in this direction is made in Table 3 which summarizes the most important non-dimensional parameters.

Table 3. Non-dimensional parameters for the flow and sand transport under different waves above rippled and plane beds

Non dimension parameter	**Description**
relative orbital diameter	d_0/d_{50}
relative ripple height	η_r/d_{50}
Reynolds number related to orbital diameter	$\mathrm{RE}_{d_0} = \frac{\hat{u}_c d_0}{\nu}$
sediment mobility	$\theta_{2.5} = \frac{1}{2} f_{2.5} \psi$
normalized sediment diffusivity	$\varepsilon_s/U k_s$
normalized height above sea bed	z/k_s
ripple steepness	η_r/λ_r
wave asymmetry	$\hat{u}_c/\hat{u}_t$
rel. water depth	h/H
rel. water depth	h/L
Wave steepness	H/L

$f_{2.5}$: Friction factor based on Swart's Formula (1974)
$\psi = (A_w\omega)^2/(s-1)gd$: Mobility number

Concluding remarks

First, the results of a comparative analysis of the suspended sediment concentration recorded using mechanical (TSS), optical (Optical Turbidity Meter) and acoustical devices (ABS) under non-breaking regular and irregular waves were discussed. It was found that the non-intrusive acoustical backscattering method (ABS) clearly represents the most appropriate device to capture the sediment entrainment event with sufficient temporal and spatial accuracy, especially above a rippled bed under non-breaking and near breaking waves. Second, a detailed analysis of the suspended sediment entrainment above a rippled bed and a plane bed in a low- and in a high-energy oscillatory flow regime, respectively, was performed, including the calculation and modeling of the sediment diffusivity profiles by means of the ABS- data set. Overall, the results have contributed to a better understanding of the temporal variation of the sediment entrainment processes above different sea bed formations in different flow regimes.

The analysis of the high resolution sound images of SSC above rippled bed has shown that due to the off-shore directed shedding process of the sediment-rich vortices generated at the on-shore flank of the steep 2D ripple and due to the phase lag between the vortex generation and the time of the flow reversal, the net sediment flux above sea beds covered with steep vortex ripples is off-shore directed. In contrast, above dynamically plane beds under near breaking wave conditions, due to the absence of the ripples and the wave asymmetry, the major sediment transport is on-shore directed and corresponds to sheet flow.

Moreover, the sediment concentration behaviour above plane bed has shown that the variation in the sediment entrainment is only weakly time dependent. The results of the highly resolved temporal and spatial structure of suspended sediment concentration above ripples have shown that the generation of the coherent sediment-rich vortices at the lee side of the steep ripple crests, which occur in a layer close to the ripple crest with the thickness of about 2-3 ripple height (Layer 1 shown in Fig. 6-a), represents the primary entrainment mechanism of the sand particles above ripples. The sediment diffusivity profiles calculated with the ABS-data set have also revealed a constant sediment diffusivity in a layer with the same height above the ripple crest. Above this layer (within layer 2 shown in Fig. 6-a), where the coherent motions break down and the turbulent processes dominate, the sediment-rich vortices are shed at the time of the flow reversal and the sand clouds are entrained to considerably higher elevations, which can be explained with the linear increase of the sediment diffusivity within the layer 2 (Fig. 6-a).

Acknowledgements
The experiments are partly supported by the European Community within the Sixth Framework Program as a part of the Joint Research Activity "SANDS", in the Integrated Infrastructure Initiative HYDRALAB III and partly by the BMBF supported project "ModPro" (03KIS060).

References

Ahmari, A., Gruene, J., Oumeraci, H. (2008) "Large scale laboratory measurement of suspended sediment concentration induced by non-breaking waves with acoustic backscatter technique," *Proc. on App. of Phy. Mod., Coastlab'08*, Bari, Italy, 93-105.

Ahmari, A. and Oumeraci, H. (2010) "Measurement and analysis of the suspended sediment concentration by waves in a rippled bed regime," *9st Int. Conf. on Coasts, ports and marine structures* (*ICOPMAS-2010*), *Teheran, Iran*.

Davies, A. G., Villaret C. (1997) "Oscillatory flow over rippled beds: boundary layer structure and wave-induced Eulerian drift," In: Gravity waves in water of finite depth, *Comp. Mec. Pub.* edited by J. N. Hunt, , 215-254.

Davies A. G., Thorne, P. (2008) "Advances in the study of monitoring and evolving seabeds," *Surv. Geophys 29.1-36.*

Nielsen, P. (1992) "*Coastal Bottom Boundary Layers and Sediment Transport, Advanced series on Coastal Engineering*," - Volume 4, World Scientific.

Swart, D. H. (1974) "*Offshore sediment transport and equilibrium beach profiles*," Delft Hydr. Lab. Publ. 131.

Soulsby, R., (1997) "*Dynamics of marine sands*", Thomas Telford Services Ltd.

Thorne, P. D., Davies, A. G. and Bell, Paul S.(2009). "Observations and analysis of sediment diffusivity profiles over sandy rippled beds under waves," *J. Geophys. Res.* Vol. 114 C02023, 1-16.

Thorne, P. D., Hanes D. M. (2002) "A review of the application of acoustic measurement to small scale sediment processes," *Cont. Shelf Res.*, 22(4) 603–632.

Thorne, P. D., Davies A. G., Williams J. J. (2003) "Measurements of near bed intra-wave sediment entrainment above vortex ripples," *Geophys. Res. Lett.*, Vol. 30, No. 20, 2028, OCE 2-1 - 2-4.